



Gas Seepage Under Continuous and Step Loading Based on True Triaxial Seepage Test Apparatus

Y. Zhang^{1,2} · J. Zhang¹ · W. Du^{1,2} · H. Wang¹ · K. Niu¹

Received: 25 January 2020 / Accepted: 6 November 2020 / Published online: 8 January 2021
© The Society for Experimental Mechanics, Inc 2021

Abstract

The conventional triaxial loading in gas seepage studies does not reflect the actual stressing state in the coal seam. Thus, a true triaxial seepage experimental apparatus is developed before seepage tests are conducted with it. The first group of tests is carried out with continuous axial loading under uniform lateral constrain on moulded coal specimen: one test under constant-velocity axial loading, two tests under monotonic variable-velocity axial loading, and two tests under single-cycle variable-velocity axial loading. The tests reflect the multi-step, discontinuous, stressing condition with variable-loading rate and strength in a coal seam. The law of coal deformation and gas permeability variation under constant-velocity and variable-velocity axial loading is obtained. Then, the multi-step seepage tests under different non-uniform lateral pressures are conducted, focusing on permeability variation under different triaxial stresses versus gas pressure and intermediate principal stress. The permeability increase with gas pressure decrease is confirmed and interpreted. Moreover, the turning point between Klinkenberg effect and gas wedging effect in the coal seam is determined. A simplified concept of average effective stress is put forward, and the dominant influence of this average effective stress on coal seam permeability is identified based on the concept.

Keywords True triaxial · Intermediate principal stress · Average effective stress · Gas seepage

Introduction

The mine gas is a major safety concern in the coal mine in forms of excess gas accumulation, coal and gas outburst, and gas explosion [1, 2]. The coal permeability is a basic parameter in the study of gas migration and flows in coal. It is also related to gas dynamics and its prevention in coal mining, coal bed methane mining, and gas extraction [3–5].

At present, the experimental research on the change law of coal permeability has made great achievements [6, 7]. Since 1970s, some scholars have developed the gas seepage test equipment and carried out related researches. W. J. Sommerton [8] has carried on the preliminary research to the influence of stress on

permeability of coal; C. R. McKee [9] has made a research of the relationship between stress and porosity and permeability of coal on the basic of W. J. Sommerton's research; Tan Xueshu [10–12] studied the change law of coal samples' permeability in different stress, temperature and deformation process; Lin Baiquan [13, 14] studied the relationship between pore pressure of gas bearing coal and permeability as well as pore pressure and coal sample deformation by means of self-developed gas permeation test device for coal samples; S. Harpalani [15, 16] studied the influence law of gas pressure on permeability through the triaxial rock mechanics test system; J. R. E. Enever and A. Henning [17] studied the influence law of effective stress on permeability of coal; Liu Jian and Liu Xiangui [18, 19] used self-made test equipment to study porous media with low permeability and the curves of porosity and permeability with effective pressure were obtained by experiments; Liu Yubing [20] measured the anisotropic permeability data under true triaxial stress conditions which were well expressed by an exponential equation containing different mean cleat compressibility and stress terms. Tang Jupeng [21] has studied the relationship between effective stress and desorption and seepage characteristics of coalbed methane; Wei Jianping, Wang Dengke and Wang Gang [18, 22–24] have made the experimental platform of

✉ W. Du
duwenzhou-01@163.com

¹ College of Safety and Environmental Engineering, Shandong University of Science and Technology, Qingdao 266590, People's Republic of China

² Key Laboratory of Ministry of Education for Mine Disaster Prevention and Control, Shandong University of Science and Technology, Qingdao 266590, People's Republic of China

seepage characteristics of coal, and studied the effect of temperature, effective stress and water content on the permeability of coal. But in the actual situation, the stress of coal is in three directions. It is of great significance to study the seepage law of coal under the three-dimensional stress for gas prevention and development of coal-bed methane. The above-mentioned physical experiments have promoted the research on deformation/failure of coal/rock and gas seepage. Due to the lateral pressure interference and gas sealing issues in the true triaxial test, the gas seepage physical experiment is usually conducted with the conventional triaxial loading and the true triaxial mechanic test under open conditions, which cannot reflect the unequal stressing in different directions and the gas occurrence in the gas-bearing coal seam. In addition, when the ratio of pore pressure to volume stress is small, the gas permeability of porous materials decreases with the increase of pore gas pressure; In this case, as the thickness of the molecular gas layer on the surface of the pores and fractures increases, the effective seepage channels decreases, which is manifested as the increase of the gas molecule migration resistance and the obvious slowdown of gas flow speed. This phenomenon is called the Klinkenberg effect. The Klinkenberg effect is very obvious to low-permeability coal, and it will become more significant as the coal absolute permeability decreases, which indicates the Klinkenberg effect is a key factor in the research of coal permeability. However, the Klinkenberg effect has been little considered in most of the above studies.

Therefore, based on previous studies, a true triaxial seepage experimental apparatus is developed in-house, and the various seepage tests under uniform and non-uniform lateral pressure

are conducted, to study the characteristics of coal strain and gas seepage under different triaxial stress conditions.

Experimental Apparatus, Material, and Test Design

Experimental Apparatus

As shown in Fig. 1, a true triaxial seepage test apparatus consists of specimen clamping pressure chamber, power and servo monitor system, and gas supply system; the top view of the true triaxial pressure chamber shows the process of specimen installing. Its specifications are listed in Table 1.

Consisting of the sealed removable pressure cylinder and the internal clamber, the specimen clamping pressure chamber is the main place for the specimen to bear load and gas seepage. As shown in Fig. 2, the axial stress σ_1 is applied with the upper hydraulic cylinder, the lateral pressure σ_2 is simultaneously applied with two laterally symmetric hydraulic cylinders, and lateral pressure σ_3 is provided by high-pressure hydraulic oil in the pressurized specimen clamping chamber. In order to avoid the interaction between σ_1 and σ_2 in the process of simultaneous loading, the press head of σ_2 is made of both rigid (stainless steel) and flexible (macromolecular resin) pressing blocks of appropriate dimensions. So that when the press head of σ_1 moves, the press head of σ_2 moves upward or downward synchronously to avoid crash through the coordination of rigid and flexible blocks.

Fig. 1 True triaxial seepage test apparatus

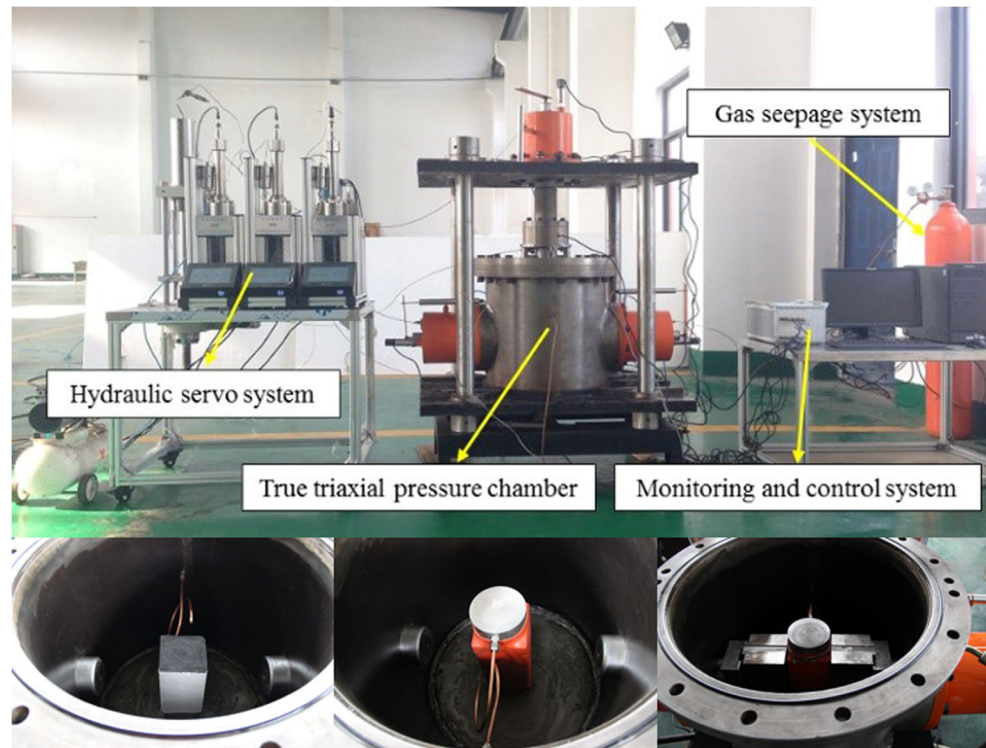


Table 1 Technological indexes of true triaxial seepage test apparatus

σ_1 (MPa)	σ_2 (MPa)	σ_3 (MPa)	Maximum gas pressure (MPa)	Maximum axial displacement (mm)	Maximum lateral displacement (mm)	Method of controlling σ_1 , σ_2 loading	Method of controlling σ_3 loading
70	35	10	6	50	30	Pressure control Displacement control	Pressure control

The power and servo monitor system consists of a hydraulic cylinder and a constant-velocity and constant-pressure metering pump. The metering pump can work in either constant-flow rate or constant-pressure mode. The servo system controls the operation of pump, with smooth, precise low noise transmission. Via the standard data interface, the technical parameters of constant-flow rate and constant pressure metering pump, e.g., pressure, flow rate, intake and output volume, are automatically collected by a computer in real time.

The gas supply system consists of high pressure gas cylinder, pressure reducing valve, and gas supply line. The reducing valve has the gas supply pressure between 0 and 6 MPa and effective aeration inside diameter of 6 mm. The gas is eventually discharged out of the laboratory.

Material

A custom mould, which includes shell, liner, base, and molding compression bar, is designed. The shell is main stressed component with split half parts. The liner is made of four smooth thin-steel sheets and is embedded into the shell. The shell has a demolding tap, through which the specimen is demolded with the bolt to avoid the damage by bottom demolding with compression machine. The steps of molding coal specimens are shown in Fig. 3.

All coal specimens are collected from the 3[#] Anthracite seams in the east area of Sihe Mine of Shanxi Jincheng Anthracite Coal Mining Group. Sihe Mine is a high gas and outburst mine. The gas pressure and content of 3[#] anthracite seams are 16.7 m³/t and

0.2 ~ 2.32 MPa, respectively. The parameters of its consolidating coefficient, initial speed of methane diffusion, adsorption constant and proximate analysis are shown in Table 2.

The raw coal sample was smashed in the grinder. The smashed coal was screened with the standard screen. 2.55 kg of 20/40 mesh and 40/80 mesh coal fines (1:1) was evenly mixed with 0.18 kg of distilled water and compressed for 30 min in a 100 t press machine (molding pressure 100 MPa). Several cuboid molded coal specimens were obtained after demolding. The specimens were placed in 80 °C drying oven for 24 h before taken out and wrapped up with cling film. The specifications of molded coal specimens are listed in Table 3.

Test Design

At present, physical experiments on coal gas seepage are usually operated under constant axial loading rate, which does not reflect the multi-step, discontinuous stress with non-uniform loading rate and strength of coal seam. In order to simulate the pressure variation and further investigate the gas seepage in the mining coal, the experiments are conducted with both constant-velocity and variable-velocity axial loading.

The above two groups of experiments were designed with five stress paths from 1 to 1[#] to 1–5[#]. Before the loading test, gas with a pressure of 1 MPa was introduced. When the gas was absorbed to balance, the true triaxial seepage test would be conducted. Firstly, the σ_1 , σ_2 and σ_3 were alternatively increased to 6 MPa hydrostatically with a loading rate of 0.01 MPa/s [25].

Fig. 2 Schematic of specimen clamping pressure chamber

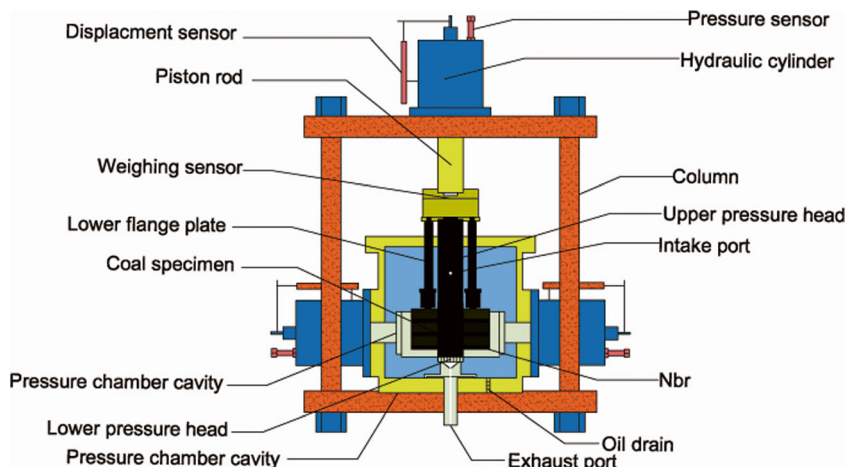
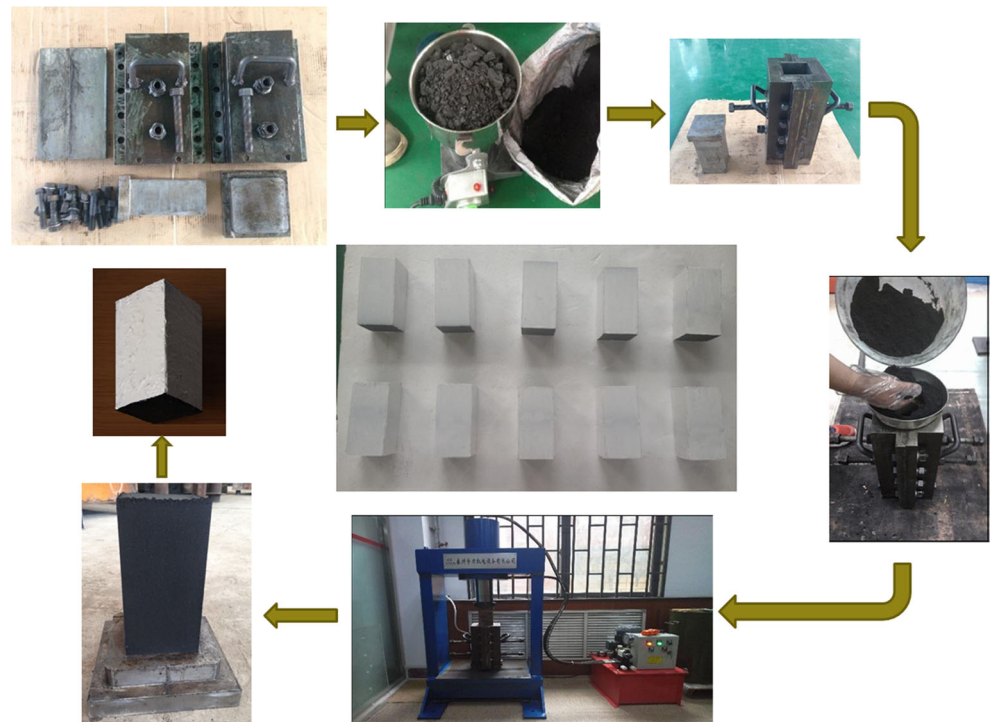


Fig. 3 Steps of moulding coal specimens



Then, the stress of σ_2 and σ_3 remained unchanged, while the seepage of spacemen was tested by changing the loading of σ_1 .

(1) Constant-velocity axial loading test

The axial stress is applied at constant axial loading velocity of 0.1 mm/min until Specimen 1–1[#] is damaged, while the gas seepage test is conducted. The maximum axial stress of 261.7kN (compressive strength of 26.17 MPa) provides reference for design of variable-velocity axial loading path.

(2) Variable-velocity axial loading test

As shown in Fig. 4, the axial stress is applied on Specimen 1–2[#] by monotonic step loading at 0.1 mm/min, 0.15 mm/min, 0.2 mm/min, 0.25 mm/min, and 0.3 mm/min, with step target values of 10 MPa, 14 MPa, 18 MPa, and 22 MPa. The stress stays at each target value (stabilization) for 5 min. The test goes on until Specimen 1–2[#] is damaged. Specimen 1–3[#] goes through an opposite step down sequence.

As shown in Fig. 5, the axial stress is applied on Specimen 1–4[#] by step loading at 0.1 mm/min, 0.2 mm/min, and

0.3 mm/min, 0.2 mm/min, and 0.1 mm/min with step target values of 10 MPa, 14 MPa, 18 MPa, and 22 MPa. The stress stays at each target value (stabilization) for 5 min. The test goes on until Specimen 1–4[#] is damaged. Specimen 1–5[#] goes through an opposite step loading sequence.

The above experiments supplement the present constant loading rate test study and serve as a starting point for studies of specimen behavior under true triaxial loading conditions, which are different from seepage test on the loaded cylindrical specimen. In order to investigate the seepage in the coal under $\sigma_2 \neq \sigma_3$, tests are conducted by stepping up the loading, i.e., the servo metering pump is set to constant-pressure mode to avoid the irreversible damage during unloading. Five tests are designed as follows.

(3) Lateral step loading test

The spacemen 2–1[#] is applied the hydrostatic pressure until the three-dimensional stress σ_1 , σ_2 and σ_3 reached 2 MPa (namely $\sigma_1 = \sigma_2 = \sigma_3 = 2$ MPa); σ_1 is maintained at 5 MPa, while σ_2 is increased to 3 MPa, 4 MPa, and 5 MPa respectively, with 5 min stabilization at each target value. In each stress

Table 2 Parameters of specimen from the east area of Sihe Mine

Hardness coefficient / <i>f</i>	Initial speed of methane diffusion / ΔP	True relative density / ($\text{g}\cdot\text{cm}^{-3}$)	Adsorption constant		Proximate analysis		
			<i>a</i> / ($\text{cm}^3\cdot\text{g}^{-1}$)	<i>b</i> / MPa^{-1}	<i>M</i> _{ad} / %	<i>A</i> _{ad} / %	<i>V</i> _{ad} / %
1.80	22.50	1.56	48.276	1.302	3.63	17.31	7.15

Table 3 Specifications of moulded coal specimens

Specimen number	Length (mm)	Width (mm)	Height (mm)
1-1 [#]	96.54	99.53	200.43
1-2 [#]	98.49	100.12	199.32
1-3 [#]	100.16	99.54	199.54
1-4 [#]	99.35	99.37	199.36
1-5 [#]	99.98	100.23	200.72
2-1 [#]	100.06	99.53	200.17
2-2 [#]	100.32	100.01	200.05
2-3 [#]	100.17	100.21	199.76
2-4 [#]	99.88	99.97	200.34
2-5 [#]	100.34	99.89	200.07

loading stage, the gas pressure is maintained at 0.5 MPa, 1.0 MPa, and 1.5 MPa in three cases, respectively.

As shown in Table 4, the true triaxial seepage tests are conducted on Specimen 2-2[#]-2-5[#] in the way similar to that on Specimen 2-1[#]. Firstly, $\sigma_1 = \sigma_2 = \sigma_3$ are increased to the target value of σ_3 hydrostatically; σ_1 is then increased to and maintained at its target value; σ_2 is increased to target values, where it stays for 5 min. In each stress loading stage, the gas pressure is maintained at 0.5 MPa, 1.0 MPa, and 1.5 MPa, 2.0 MPa and 2.5 MPa, respectively.

Results and Discussion

This study assumes that laboratory room temperature is constant, moulded coal specimen is isotropic, homogeneous materials, and gas flow is slow (Darcian flow). From the measured gas pressure and flow rate, the coal’s permeability under the corresponding stress can be calculated as below [26]:

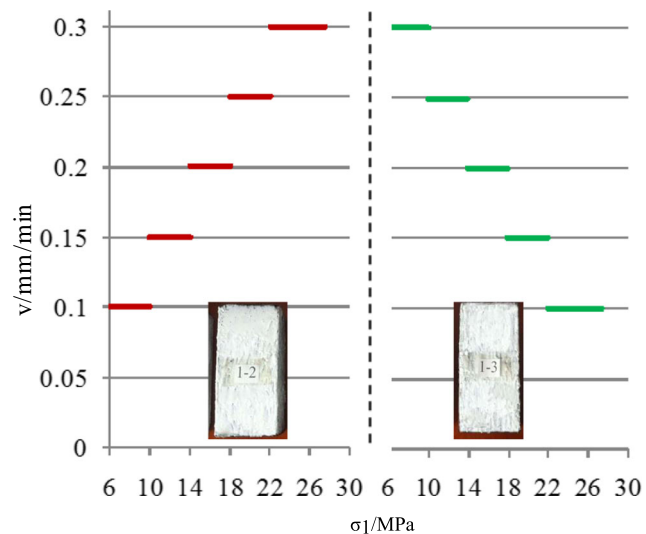


Fig. 4 Monotonic variable-velocity loading test plan

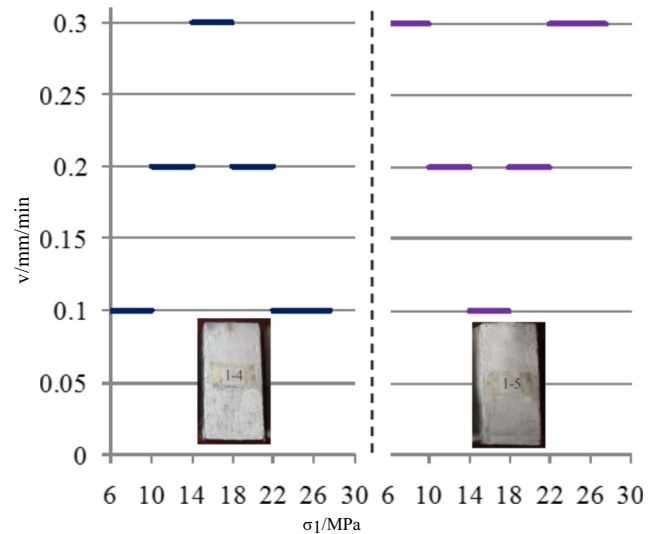


Fig. 5 Single-cycle variable-velocity loading test plan

$$K = \frac{2q\mu LP_n}{A(P_2^2 - P_1^2)} \tag{1}$$

where K denotes coal’s permeability in m^2 ; q denotes the coal’s seepage velocity in m^3/s ; μ denotes the gas’s kinetic viscosity coefficient and is generally set as 1.10×10^{-11} MPa*s for CH₄; L denotes the coal specimen’s length in m; P_n denotes the barometric pressure and IS set as 0.1 MPa; A denotes the specimen’s cross-sectional area in m^2 ; P_1 and P_2 are the gas pressures at the intake and the outlet, respectively, in MPa.

Gas Seepage characteristics under Constant-Velocity and Variable-Velocity Axial Loading

The influencing factors in gas seepage are complicated. They are closely related to coal pore structure, gas pressure, gas content, gas adsorption/desorption characteristics, coal seam temperature, and water content in the coal [27]. As other initial conditions are constant, the coal seam permeability under different axial loading conditions is mostly related to pore structure, and the relationship is expressed as strain versus seepage. In this study, no rigid stress is applied for the intermediate principal stress, which is equal (in magnitude) to the small principal stress ($\epsilon_2 = \epsilon_3 = (\epsilon_2 + \epsilon_3)/2$). Both stresses are applied though the high hydraulic oil inside the pressurized specimen clamping chamber.

The curves of strain and permeability versus time under different stressing paths are shown in Fig. 6(a)–(c). The analysis shows the following results:

- (1) Compared with the test with constant-velocity axial loading, the coal seam permeability versus loading rate curve under variable-velocity axial loading is obviously stepped. In stable pressure stages AB, CD, EF, and

Table 4 Target values for step loading

Coal specimens	σ_1 (MPa)	σ_2 (MPa)	σ_3 (MPa)	Gas(MPa)
2-1 [#]	5	2, 3, 4, 5、	2	0.5, 1.0, 1.5、
2-2 [#]	10	3, 5, 7, 9, 10	3	0.5, 1.0, 1.5, 2.0, 2.5
2-3 [#]	15	4, 7, 9, 11, 13, 15	4	0.5, 1.0, 1.5, 2.0, 2.5
2-4 [#]	20	5, 9, 13, 17, 20	5	0.5, 1.0, 1.5, 2.0, 2.5
2-5 [#]	25	6, 11, 16, 21, 25	6	0.5, 1.0, 1.5, 2.0, 2.5

GH, the subtle change in the micro-fissures and pores inside the coal is a result of stress-strain lag, which is ignored in later analysis.

- (2) In the early loading stage (OA and BC, where the axial stress increases from 6 MPa to 14 MPa), for Specimens 1-2[#]-1-5[#]: when the loading rate in Specimen 1-2[#] increases from 0.1 mm/min to 0.15 mm/min, the permeability variation rate increases from 9.5×10^{-4} mD/s to 14.6×10^{-4} mD/s; when the loading rate on Specimen 1-3[#] decreases from 0.3 mm/min to 0.25 mm/min, the permeability variation rate decreases from 9.47×10^{-4} mD/s to 8.45×10^{-4} mD/s; when the loading rate on Specimen 1-4[#] increases from 0.1 mm/min to 0.2 mm/min, the permeability variation rate increases from 7.26×10^{-4} mD/s to 9.22×10^{-4} mD/s; when the loading rate on Specimen 1-5[#] decreases from 0.3 mm/min to 0.2 mm/min, the permeability variation rate decreases from 19.82×10^{-4} mD/s to 15.14×10^{-4} mD/s. In the early loading stage, the open structural planes and fissures inside the coal grains deform, and the macro-fissures are compressed. This helps to reduce the gas migration channels, which, combined with gas adsorption, would result in a loss of permeability. The data analysis indicates that in this stage loading rate is the dominant factor with a significant inverse correlation between the permeability change rate and the axial stress loading rate.
- (3) In the middle stage of loading (DE and FG, where the axial stress increases from 14 MPa to 22 MPa). For Specimens 1-2[#]-1-5[#], one sees: when the loading rate on Specimen 1-2[#] increases from 0.2 mm/min to 0.25 mm/min, the permeability variation rate decreases from 10.4×10^{-4} mD/s to 5.2×10^{-4} mD/s; when the loading rate on Specimen 1-3[#] decreases from 0.2 mm/min to 0.15 mm/min, the permeability variation rate decreases from 7.74×10^{-4} mD/s to 4.87×10^{-4} mD/s; when the loading rate on Specimen 1-4[#] decreases from 0.3 mm/min to 0.2 mm/min, the permeability variation rate decreases from 3.58×10^{-4} mD/s to 2.77×10^{-4} mD/s, and when the loading rate on Specimen 1-5[#] increases from 0.1 mm/min to 0.2 mm/min, the permeability variation rate decreases from 9.1×10^{-4} mD/s to 3.84×10^{-4} mD/s. In the middle stage of loading, the continuing compression leads to distributed damage in the coal, as well as steady extending and further

development of seepage pores. Meanwhile, as the gas concentration gradient drives the gas molecules diffusion from the seepage pores to the adsorption pores. The pore and fissure deformation resulted from gas adsorption reduce the permeability. The data analysis shows that in this stage gas adsorption is the dominant factor for permeability variation rate, which decreases regardless of the axial loading rate. There must be a turning point in the relation between the permeability variation rate and the loading rate.

- (4) In the late loading stage (from point H until the end of test), both axial and lateral strain rapidly increase. The micro-fissures continue to propagate and increase under axial stress, but at a much slower rate. The reduced gas adsorption in the coal leads to a stabilizing permeability variation rate.

The study on the strain versus permeability curves in Fig. 7(a)-(e) reveals an inverse correlation between the permeability K and the axial strain ε_1 . As the axial stress increases, the lateral strain ε_3 increases, and the permeability decreases correspondingly. Within elastic range (before the volume strain ε_v decreases), as the coal volume decreases under axial stress loading, the fissures and pores inside the coal decrease, resulting in an inverse correlation between permeability and volume strain. In the late stage of decreasing volume strain ε_v , as the lateral strain becomes greater than axial strain, the volume strain turns negative, resulting in a stabilized permeability. All these above observations are valid before macro fissures are generated in the specimen.

Seepage Characteristics of Gas under Step Loading

According to the plan, the tests are conducted by stepping up the loading on the specimens under different lateral pressure, and the coal specimen permeability in different stages is obtained. The results of permeability variation rate versus gas pressure under different triaxial stresses are shown in Fig. 8(a)-(e), where different curves correspond to different values of σ_2 .

- (1) During the loading step-up, as the gas pressure increases, the permeability of coal seam specimen exhibits different tendencies. For Specimen 2-1[#], the permeability decreases. For Specimen 2-2[#], the permeability goes down and up. When the intermediate principal stress is below 10 MPa,

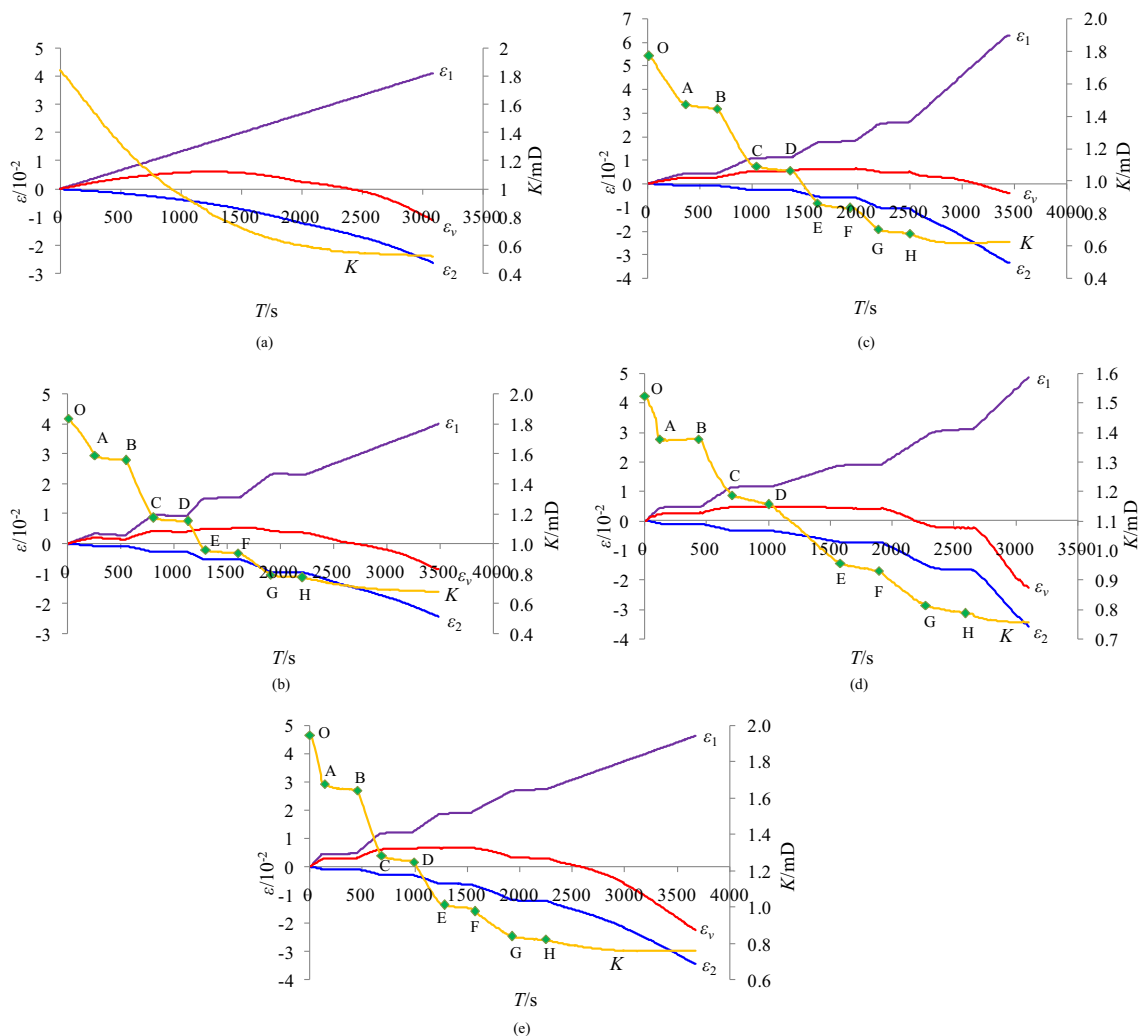


Fig. 6 Curves of strain and permeability versus time. Figure 6(a) ~ Figure 6(e) are the strain and permeability curves of five specimens under different loading rates. The four curves in each figure show Permeability K , axial strain ε_1 , lateral strain ε_2 and volumetric strain ε_v , respectively. The curves in Figure 6(a) shows the results of specimen 1-1[#] under a constant axial loading rate of 0.1 mm/min; Figure 6(b) to Figure 6(e) show the status

of specimens being applied gradually increasing or decreasing loading rate (seeing Figures 4 and 5 for details of loading rates). The small green squares divide the gradual loading process into three stages: early stage (OA section and BC section), middle stage (DE section and FG section), and late stage (post H point stage).

the turning point of permeability occurs at gas pressure = 1 MPa. When the intermediate principal stress is 10 MPa, the turning point of permeability occurs at gas pressure = 1.5 MPa. For Specimen 2-3[#], when the intermediate principal stress is 4 MPa, as the gas pressure increases, the permeability increases; and when the intermediate principal stress is over 4 MPa, the permeability does down and up, which is consistent with the case of Specimen 2-2[#]. For Specimens 2-4[#] and 2-5[#], the permeability increases monotonically as the gas pressure increases.

Thus, it can be seen that with lower effective stress, as the gas pressure increases, the coal permeability does not increase monotonically, but decreases before increases later. This well explains the reduced Klinkenberg effect at higher gas pressure

[28, 29], i.e. the reduced slip flow of gas molecule at high pressure on the solid plane promotes the gas adsorption, and the swelled coal grains reduces the effective porosity and permeability. When the gas concentration reaches a certain value, the gas adsorption is stabilized, and the wedging effect by gas becomes dominated, which gives rise to an increase in permeability. Our test result indicates that the turning point (in gas pressure) between Klinkenberg effect and the gas wedging effect lies somewhere between 1 MPa and 1.5 MPa.

- (2) With constant σ_1 , σ_3 , and gas pressure, the coal permeability variation is affected by the rigid loading of σ_2 . Generally, large σ_2 tends to reduce coal permeability, because before failure occurs an increasing σ_2 increases the coal effective stress, which reduces gas permeability

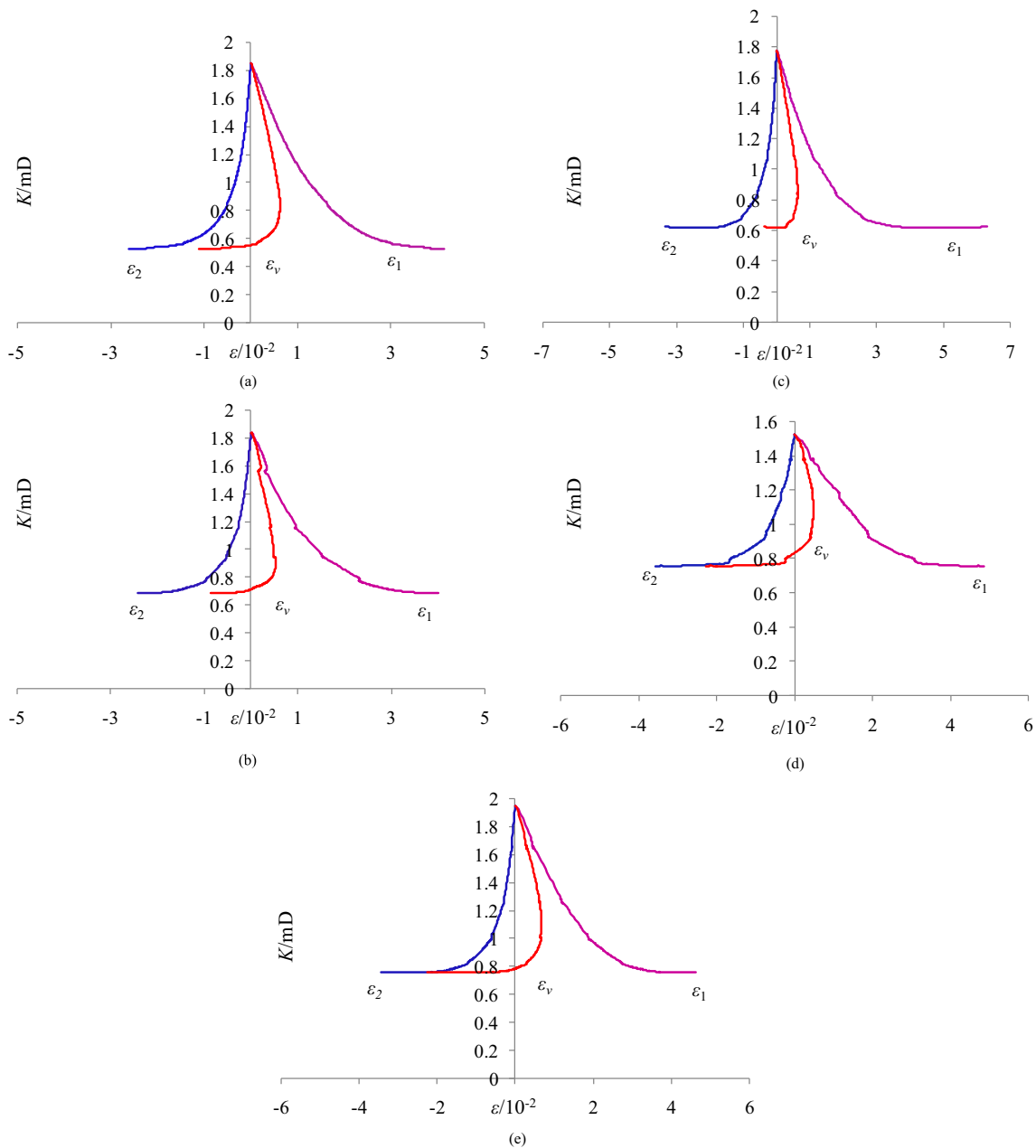


Fig. 7 Curves of permeability versus strain. Figure 7 shows the relationship between the permeability and strain of five specimens at their loading rates in the Constant-velocity loading test and the variable-velocity loading test. The ordinate is the permeability and the abscissa is the strain. Figure 7(a) shows the permeability of specimen 1-1[#] with the

change of axial strain ϵ_1 , lateral strain ϵ_3 , and volumetric strain ϵ_v in the constant-velocity loading test; Figure 7(b) to Figure 7(e) show the results of specimen 1-2[#], specimen 1-3[#], specimen 1-4[#], and specimen 1-5[#] at four different loading rates in the variable-velocity loading test.

by condensing the pore-fissure structure and blocking gas seepage channels. This is elaborated as follows.

As the coal is a porous medium, its skeleton is influenced by stress of different directions and pore pressure. For true triaxial loading, the average effective stress [30, 31] is expressed in Formula 2, where σ is the average effective stress. The obtained permeability versus average stress curves in different specimens are shown in Fig. 9.

$$\sigma = \frac{1}{3}(\sigma_1 + \sigma_2 + \sigma_3) - \frac{1}{2}(p_1 + p_2) \quad (2)$$

As shown in Fig. 9, with other conditions unchanged, the permeability of moulded coal specimen decreases as the effective stress increases, which is possibly due to the condensation of the structure. The large slope also indicates the dominance of the average effective stress as the major influencing factor on permeability. This is similar to the conclusions of Ye

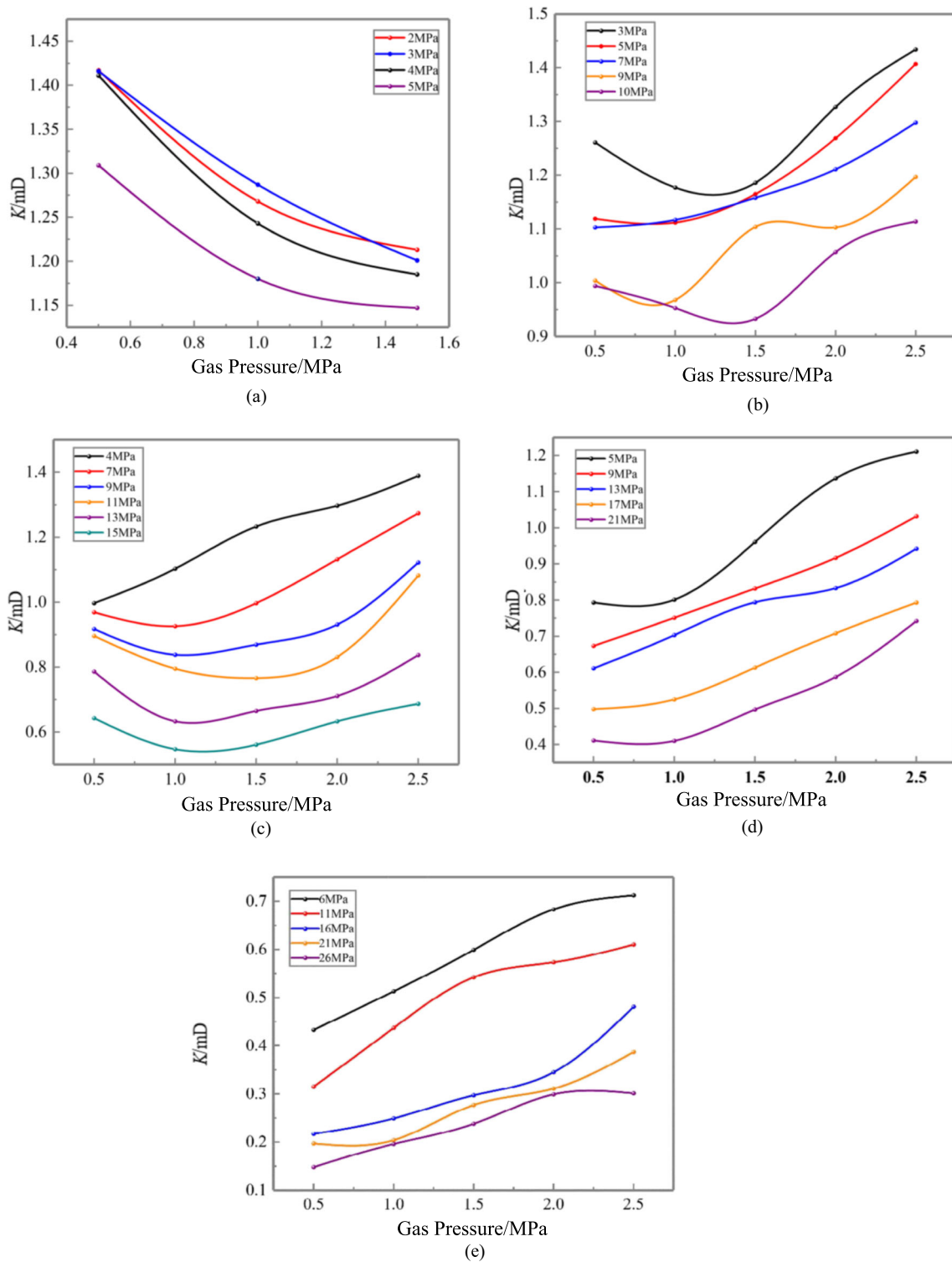


Fig. 8 Curves of permeability versus gas pressure under different triaxial stress conditions. Figure 8 shows the permeability variation of specimen with the increase of gas pressure under five different three-dimensional stress conditions. The axial stress σ_1 in Figure 8(a) is 5 MPa, the lateral stress σ_3 is 2 MPa, and the lateral stress σ_2 is adjusted to 3 MPa, 4 MPa and 5 MPa, respectively. The abscissa represents the corresponding gas

pressure of 0.5 MPa, 1.0 MPa and 1.5 MPa for each stress loading stage. Figures 8(b) to Figures 8(e) show the permeability changes of each specimen under different three-dimensional stress paths when the gas pressure is 0.5 MPa, 1.0 MPa, 1.5 MPa, 2.0 MPa and 2.5 MPa, respectively (Seeing Table 4 for the three-dimensional stress paths).

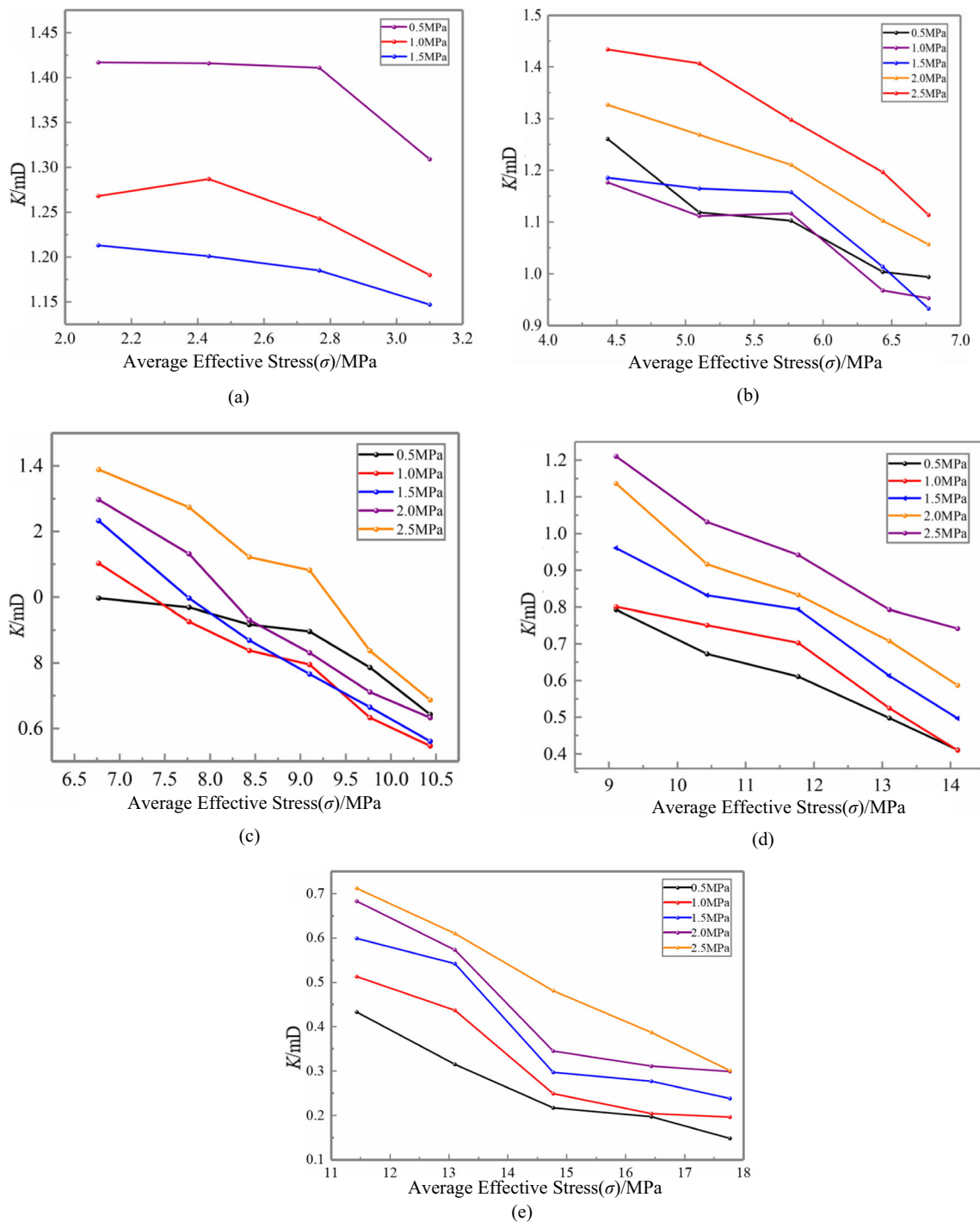


Fig. 9 Curves of permeability versus average effective stress. Figure 9(a) to Figure 9(e) shows the permeability variation with the change of average effective stress under five different three-dimensional stress

conditions, respectively. (Seeing Table 4 and Figure 8 for the three-dimensional stress paths of the five sub-figures)

Yuanxin and Xu Jiang [32, 33], the difference is that Ye Yuanxin's study is the water seepage in calcilutite rock under the true triaxial condition, Xu Jiang's research is the gas seepage in coal under the condition of false triaxial, while this paper is the innovation research of gas seepage under true triaxial continuous.

Conclusions

- (1) A true triaxial seepage test apparatus with flow-solid coupling is developed. The apparatus is applicable in the true triaxial mechanical and permeability tests of coal seam under different triaxial stresses and pore pressures.

Particularly, it provides a new approach and platform for research on gas migration and flow.

- (2) The seepage tests with constant-velocity and variable-velocity axial loading under uniform lateral pressure are conducted. In early loading stage, permeability is inversely correlated with the axial loading rate. In the middle stage of loading, the permeability variation rate decreases regardless of the axial loading rate, indicating that there is a turning point in the relation between the permeability variation rate and the loading rate. In the late loading stage, both axial and lateral strain rapidly increase, and micro-fissures continue to propagate and increase under axial stress. However, the notably slowed rate and smaller gas adsorption result in a reduced permeability variation rate.
- (3) Seepage test with lateral step loading constrained by different lateral pressures shows that as the gas pressure increases, the permeability tends to increase. However, when the effective stress is low, it does not increase monotonically, but decreases first before the increase. This is consistent with the Klinkenberg effect, and the turning point between Klinkenberg effect and gas wedging effect in coal occurs when the gas pressure is between 1 MPa and 1.5 MPa. A simplified concept of average effective stress is presented, based on which it is shown that the coal permeability is dominated by average effective stress.
- (4) The above third and four conclusions are more qualitative. In the next step, the raw coal specimens will be subjected to the continuous loading and unloading experiments under different conditions of σ_2 and σ_3 . Quantitative display of the influence of multi-direction loading and unloading on the deformation, failure and permeability of coal. Meanwhile, dynamic CT scanning and acoustic emission device are considered for equipment, numerical simulation method is combined to study fracture development and seepage characteristics under different loading conditions.

Compliance with Ethical Standards

Conflict of Interest On behalf of all authors, the corresponding author states that there is no conflict of interest.

References

1. Peng SJ, Xu J, Yang HW, Liu D (2012) Experimental study on the influence mechanism of gas seepage on coal and gas outburst disaster. *Saf Sci* 50:816–821
2. Du WZ, Wang G, Wang Y, Liu XL (2019) Thermal degradation of bituminous coal with both model-free and model fitting methods. *Appl Therm Eng* 152:169–174
3. Sun MY (2005) Current status and prospects of CBM industry in China. *China Coalbed Methane* 2(3):3–5
4. Perera MSA, Ranjith PG, Choi SK (2013) Coal cleat permeability for gas movement under triaxial, non-zero lateral strain condition: A theoretical and experimental study. *Fuel* 109:389–399
5. United Nations (1997) UNFCCC: Kyoto Protocol to the United Nations Framework Convention on Climate Change. COP3, Tokyo
6. Cao YX, He DD, Glick DC (2001) Coal and gas outbursts in footwalls of reverse faults. *Int J Coal Geol* 48(1):47–63
7. Liu Q, Nie W, Hua Y et al (2019) Research on tunnel ventilation systems: dust diffusion and pollution behaviour by air curtains based on CFD technology and field measurement. *Build Environ* 147:444–460
8. Sommerton WH, Soylemezoglu IM, Dudley RC (1975) Effect of stress on permeability of coal. *Int J Rock Mech Min Sci Geomech Abstr* 12(2):129–145
9. Mckee CR, Bumb AC, Koenig RA (1988) Stress-dependent permeability and porosity of coal and other geologic formations. *SPE Formation Evaluation* 3(1):81–91
10. Tan XS, Xian XF, Zhang GY (1994) Study on the permeability of coal. *J Xi'an Min Inst* 1:22–25
11. Liu SQ, Zhang SJ, Chen F, Wang CH, Liu MY (2014) Variation of coal permeability under dehydrating and heating: a case study of ulanqab lignite for underground coal gasification. *Energy Fuel* 28(11):6869–6876
12. Wang HT, Li XH, Xian XF, Du YG (2004) Testing study on seepage properties of methane gas in coal under the action of geoelectric field. *Chin J Rock Mech Eng* 23(2):303–306
13. Lin BQ, Zhou SN (1987) Experimental study on gas permeability of coal sample. *J China Univ Min Technol* 1:21–28
14. Peng DR (1995) Development and application of coal rock permeability measuring instrument. *Coal Mine Mach* 5:29–31
15. Harpalani S, Schraunagel RA (1991) Shrinkage of coal matrix with release of gas and its impact on permeability of coal. *Fuel* 69(5):551–556
16. Harpalani S, Chen G (1993) Gas slippage and matrix shrinkage effects on coal permeability. *Proceedings of the 1993 International Coal bed Methane Symposium* 285–294
17. Enever JRE, Henning A (1997) The relationship between permeability and effective stress for Australian coal and its implications with respect to coalbed methane exploration and reservoir model. *Proceedings of the 1997 International Coal bed Methane Symposium*, 13–22
18. Wang G, Li WX, Wang PF, Yang XX, Zhang ST (2017) Deformation and gas flow characteristics of coal-like materials under triaxial stress conditions. *Int J Rock Mech Min Sci* 91:72–80
19. Liu JJ, Liu XJ (2007) The effect of effective pressure on porosity and permeability of low permeability porous media. *J Geom* 7(1):41–44
20. Tang JP, Pan YS, Li CQ, Shi Q, Dong ZX (2006) Experimental study on effect of effective stress on desorption and seepage of coalbed methane. *Chin J Rock Mech Eng* 25(8):1563–1568
21. Liu YB, Li MH, Yin GZ, Zhang DM, Den BZ (2018) Permeability evolution of anthracite coal considering true triaxial stress conditions and structural anisotropy. *J Nat Gas Sci Eng* 52:492–506
22. Shen J, Qin Y, Wang GX, Fu XH, Wei CT, Lei B (2011) Relative permeabilities of gas and water for different rank coals. *Int J Coal Geol* 86:266–275
23. D.K. Wang, M. Peng, J.p. Wei, Q.C. Fu, Y.L. Xia, development and application of tri-axial creep-seepage-adsorption and desorption experimental device for coal. *J China Coal Soc* 2016, 41(03), 644–652
24. Xu J, Peng SJ, Yin GZ, Tao YQ, Yang HW, Wang WZ (2010) Development and application of triaxial servo-controlled seepage equipment for thermo-fluid-solid coupling of coal containing methane. *Chin J Rock Mech Eng* 29(5):907–914

25. Zhou T (2012) Experimental study seepage characteristics of coal containing methane under cyclic loads pressure. College of Resources and Environmental Science of Chongqing University, Chongqing
26. Wang G, Cheng WM, Guo H, Long QM (2012) Study on permeability Characteristics of coal Bodywith gas pressure variation. *J Min Saf Eng* 29(05):735–739
27. Sobczyk J (2011) The influence of sorption processes on gas stresses leading to the coal and gas outburst in the laboratory conditions. *Fuel* 90:1018–1023
28. Klindenberg LJ (1941) The permeability of porous media to liquids and gases. *API Drill Prod Pract* 2:200–213
29. Yin GZ (2012) Mechanism and experimental study of solid liquid gas coupling in deep coal and gas mining. Science Press, Beijing
30. Wang Z, Yuan M (2017) Sensitivity analysis of coal permeability to temperature and average effective stresses. *China Coalbed Methane* 14(4):43–47
31. Ding ZX (2017) Mechanical fundamentals of seepage force concept and its generalization. *Chin J Geotech Eng* 39(11):2088–2101
32. Ye YX, Liu GT (2007) Porous seepage in calcirudite rock with 3-D stresses. *J Tsinghua Univ (Sci Tech)* 47(3):335–339
33. Xu J, Yuan M, Li BB, Tao YQ (2012) Experimental study of relationships between metamorphic grade pore characteristics and permeability of coal. *Chin J Rock Mech Eng* 31(4):681–687

Publisher's Note Springer Nature remains neutral with regard to jurisdictional claims in published maps and institutional affiliations.

